

超新星背景ニュートリノのエネルギースペクトル計算

2015.5.15 @ 神戸大学
東京理科大学理工学部 鈴木英之
共同研究者：中里、持田、新納

Spectrum of the Supernova Relic Neutrino Background and Metallicity Evolution of Galaxies

Ken'ichiro Nakazato, Eri Mochida, Yuu Niino, and Hideyuki Suzuki
ApJ 804 (2015) 75

超新星背景ニュートリノ

過去の超新星で放出されたニュートリノが、宇宙膨張により赤方偏移しながら、宇宙空間を（ほぼ）一様に満たしているはず。

- 超新星発生率
- 個々の超新星で放出されるニュートリノのエネルギースペクトル
- 宇宙膨張則

⇒ 現在の超新星背景ニュートリノエネルギースペクトル

星によって、放出される超新星ニュートリノの量、スペクトルは異なる。
 (初期) 質量 M 、金属量 Z によって、コアの密度分布などが異なる。

$$\Rightarrow \frac{dN_\nu(E'_\nu, M, Z)}{dE'_\nu}$$

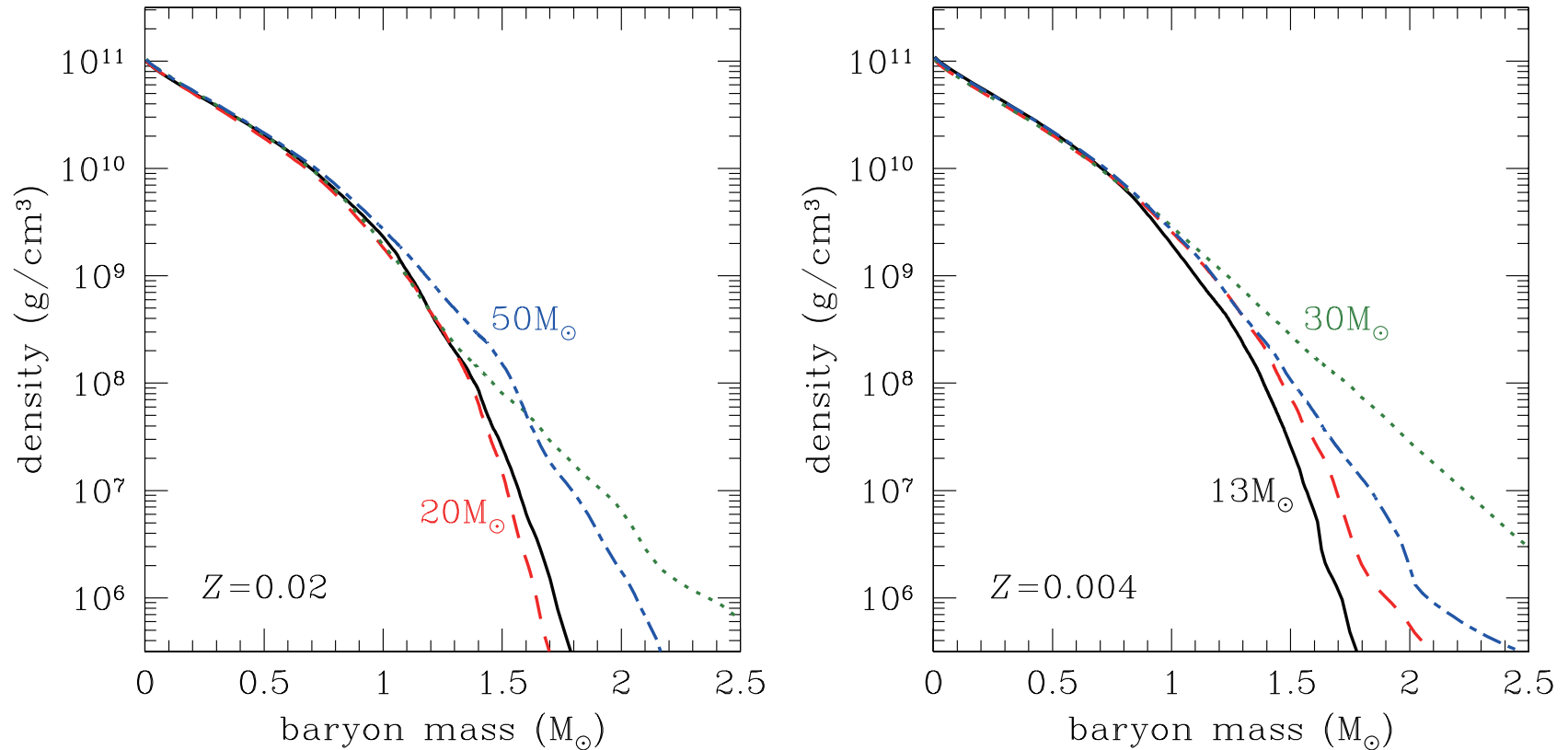


Figure 4. Density profiles at times with the central density of $10^{11} \text{ g cm}^{-3}$ for progenitor models with metallicity $Z = 0.02$ (left panel) and 0.004 (right panel). In both panels, solid, dashed, dotted, and dot-dashed lines correspond to the models with initial mass $M_{\text{init}} = 13 M_\odot$, $20 M_\odot$, $30 M_\odot$, and $50 M_\odot$, respectively. (A color version of this figure is available in the online journal.)

銀河の化学進化

- 金属は、星の内部や爆発時に作られ、超新星爆発や恒星風などでまき散らされ、次世代の星の材料となる。宇宙の平均金属量は、時間 (t あるいは赤方偏移パラメーター z) とともに増加するが、銀河によって金属量は異なる。

⇒ 星の金属量分布: $\psi_{ZF}(z, Z)$

- 星形成率 (SFR: Star Formation Rate) と金属量は相互に強く影響を及ぼす。
金属量 \Rightarrow 物質の不透明度 (Opacity) \Rightarrow SFR \Rightarrow 星の数 \Rightarrow 生成・放出される金属量

- すなわち SFR も銀河によって異なる。銀河分布と組み合わせて、宇宙平均の星形成率密度 (CSFRD: Cosmic Star Formation Rate Density) $\dot{\rho}_*(z)$ [$M_\odot \text{ yr}^{-1} \text{ Mpc}^{-3}$] を求める。

- また、生まれる星は様々な質量をもつ

⇒ 初期質量分布 (IMF: Initial Mass Function): $\psi_{\text{IMF}}(M)$

初期質量が $M \sim M + dM$ の星の形成率 [yr^{-1}] $\propto \psi_{\text{IMF}}(M) dM$

$$\text{星の重力崩壊発生率 } R_{\text{CC}}(z) = \dot{\rho}_*(z) \times \frac{\int_{M_{\text{min}}}^{M_{\text{max}}} \psi_{\text{IMF}}(M) dM}{\int_{0.1M_\odot}^{100M_\odot} M \psi_{\text{IMF}}(M) dM} [\text{yr}^{-1} \text{ Mpc}^{-3}]$$

($0.1M_\odot$ から $100M_\odot$ の星の中で、 $M_{\text{min}} = 10M_\odot$ から $M_{\text{max}} = 100M_\odot$ の星が重力崩壊するとした)

Reference model

CSFRD 宇宙星形成率密度 $\dot{\rho}_*(z)$

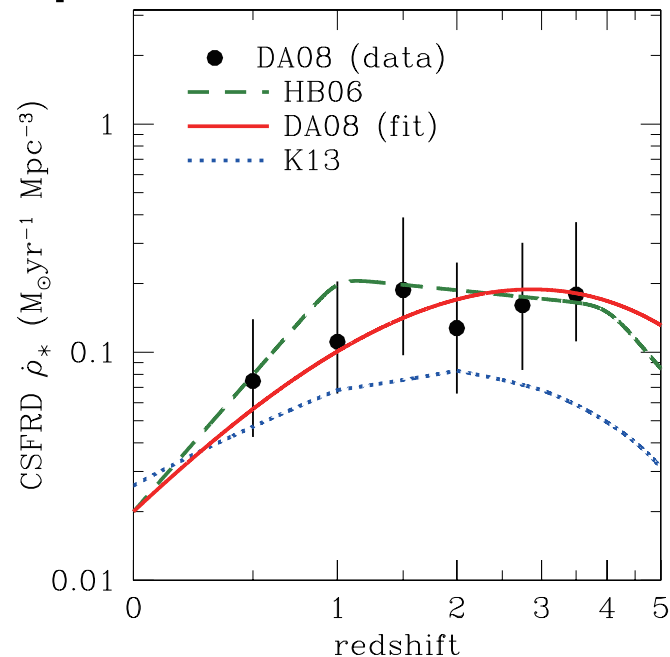
様々な星質量を持った銀河の平均 $\dot{\rho}_*(z) = \int_0^\infty \dot{M}_*(M_*, z) \phi_{\text{SMF}}(M_*, z) dM_*$

M_* : 銀河の星質量

$\phi_{\text{SMF}}(M_*, z)$: 星質量関数 (Drory & Alvarez'08)

$\phi_{\text{SMF}}(M_*, z) dM_*$: 星質量が $M_* \sim M_* + dM_*$ の銀河の数密度 [Mpc^{-3}]

$\dot{M}_*(M_*, z)$: 星質量 M_* の銀河における星形成率 (DA08 をベースに観測をフィット) [$M_\odot \text{ yr}^{-1}$]



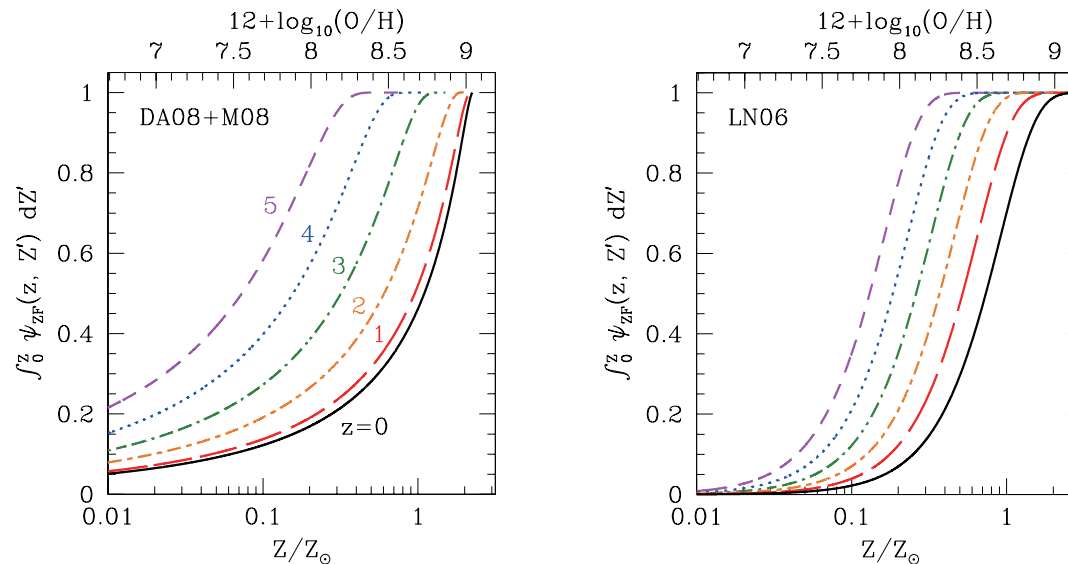
CSFRD as a function of redshift. Dashed, solid and dotted lines correspond to the models in Hopkins & Beacom'06, DA08 and Kobayashi *et al.*'13, respectively.

IMF 初期質量関数 : Salpeter 型 $\psi_{\text{IMF}}(M) \propto M^{-2.35}$

金属量分布関数 : $\psi_{ZF}(z, Z)$

銀河の星質量 (M_*) と金属量の関係 $Z(M_*, z)$ (Maiolino *et al.*'08) と、DA08 の M_* 分布を組み合わせ、赤方偏移 z の時期に生まれる星の金属量分布 $\psi_{ZF}(z, Z)$ を得る。(ただし、一つの銀河内で同時期に形成される星は同じ金属量とした)

$$\int_0^Z \psi_{ZF}(z, Z') dZ' = \frac{\int_0^{M_*(z, Z)} \dot{M}_*(M'_*, z) \phi_{SMF}(M'_*, z) dM'_*}{\int_0^\infty \dot{M}_*(M'_*, z) \phi_{SMF}(M'_*, z) dM'_*}$$



Normalized cumulative metallicity distribution function, which represents the fraction of progenitors with metallicity less than Z , for the models in DA08+Maiolino'08 (*left*) and Langer & Norman'06 (*right*). The lines correspond, from bottom to top, to redshifts of $z = 0, 1, 2, 3, 4$ and 5 .

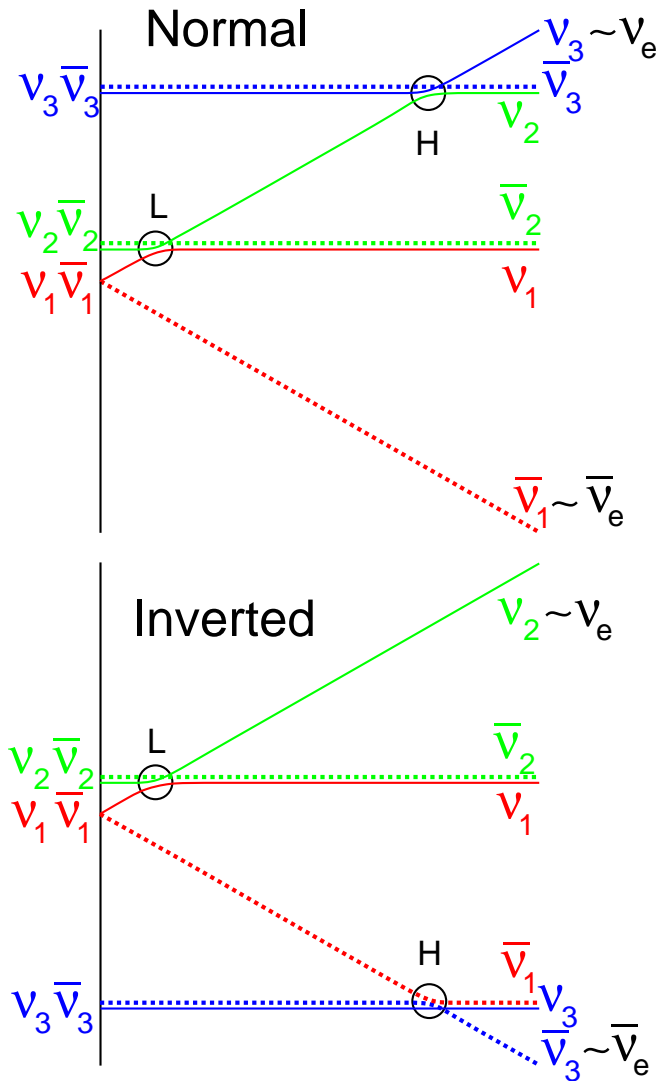
赤方偏移 z の時期に生成される星の中で、金属量が Z 以下の星の割合

$\frac{d^2 R_{\text{CC}}(z, M, Z)}{dM dZ} dZ dM$: 赤方偏移 z のとき、単位共動体積あたり金属量 $Z \sim Z + dZ$ 、
初期質量 $M \sim M + dM$ の星が重力崩壊する頻度

現在の超新星背景ニュートリノのエネルギースペクトル

$$\begin{aligned}
 \frac{dF_\nu(E_\nu, t_0)}{dE_\nu} &= c \int_0^{t_0} \int_{M_{\min}}^{M_{\max}} \int_0^{Z_{\max}} \frac{d^2 R_{\text{CC}}(z, M, Z)}{dM dZ} dZ dM \frac{dN_\nu(E'_\nu, M, Z)}{dE'_\nu} \frac{dE'_\nu}{dE_\nu} dt \\
 &\quad dt = -\frac{dz}{(1+z)H(z)}, \quad dE'_\nu = (1+z)dE_\nu \\
 &= c \int_0^{z_{\max}} \int_{M_{\min}}^{M_{\max}} \int_0^{Z_{\max}} \frac{d^2 R_{\text{CC}}(z, M, Z)}{dM dZ} \frac{dN_\nu(E'_\nu, M, Z)}{dE'_\nu} dZ dM \frac{dz}{H(z)} \\
 &\quad H(z) = \sqrt{\Omega_m(1+z)^3 + \Omega_\Lambda} H_0 \\
 &\quad \frac{d^2 R_{\text{CC}}(z, M, Z)}{dM dZ} dZ dM = R_{\text{CC}}(z) \psi_{\text{ZF}}(z, Z) dZ \psi_{\text{IMF}}(M) dM \text{ として} \\
 &= c \int_0^{z_{\max}} \frac{dz}{H_0 \sqrt{\Omega_m(1+z)^3 + \Omega_\Lambda}} \\
 &\quad \times \left[R_{\text{CC}}(z) \int_0^{Z_{\max}} \psi_{\text{ZF}}(z, Z) \left\{ \int_{M_{\min}}^{M_{\max}} \psi_{\text{IMF}}(M) \frac{dN(M, Z, E'_\nu)}{dE'_\nu} dM \right\} dZ \right]
 \end{aligned}$$

Neutrino Oscillation



$$\phi_{\nu_x} \equiv \frac{1}{4}(\phi_{\nu_\mu} + \phi_{\bar{\nu}_\mu} + \phi_{\nu_\tau} + \phi_{\bar{\nu}_\tau})$$

$$\phi_{\nu_e}^{obs}(E) = P(E)\phi_{\nu_e}^{SN}(E) + (1 - P(E))\phi_{\nu_x}^{SN}(E)$$

$$\phi_{\bar{\nu}_e}^{obs}(E) = \bar{P}(E)\phi_{\bar{\nu}_e}^{SN}(E) + (1 - \bar{P}(E))\phi_{\nu_x}^{SN}(E)$$

$$4\phi_{\nu_x}^{obs}(E) = (1 - P(E))\phi_{\nu_e}^{SN}(E) + (2 + P(E) + \bar{P}(E))\phi_{\nu_x}^{SN}(E) + (1 - \bar{P}(E))\phi_{\bar{\nu}_e}^{SN}(E)$$

Dighe and Smirnov, PRD 62 (2000) 033007

$$\begin{aligned} \frac{dN_{\bar{\nu}_e}}{dE_\nu} &= |U_{e1}|^2 \frac{dN_{\bar{\nu}_1}}{dE_\nu} + |U_{e2}|^2 \frac{dN_{\bar{\nu}_2}}{dE_\nu} + |U_{e3}|^2 \frac{dN_{\bar{\nu}_3}}{dE_\nu} \\ &= \cos^2 \theta_{12} \cos^2 \theta_{13} \frac{dN_{\bar{\nu}_1}}{dE_\nu} + \sin^2 \theta_{12} \cos^2 \theta_{13} \frac{dN_{\bar{\nu}_2}}{dE_\nu} \\ &\quad + \sin^2 \theta_{13} \frac{dN_{\bar{\nu}_3}}{dE_\nu} \end{aligned}$$

H resonance: $\rho_H \sim O(10^3) \text{g/cm}^3$ と

L resonance: $\rho_L \lesssim O(10) \text{g/cm}^3$ が adiabatic のとき

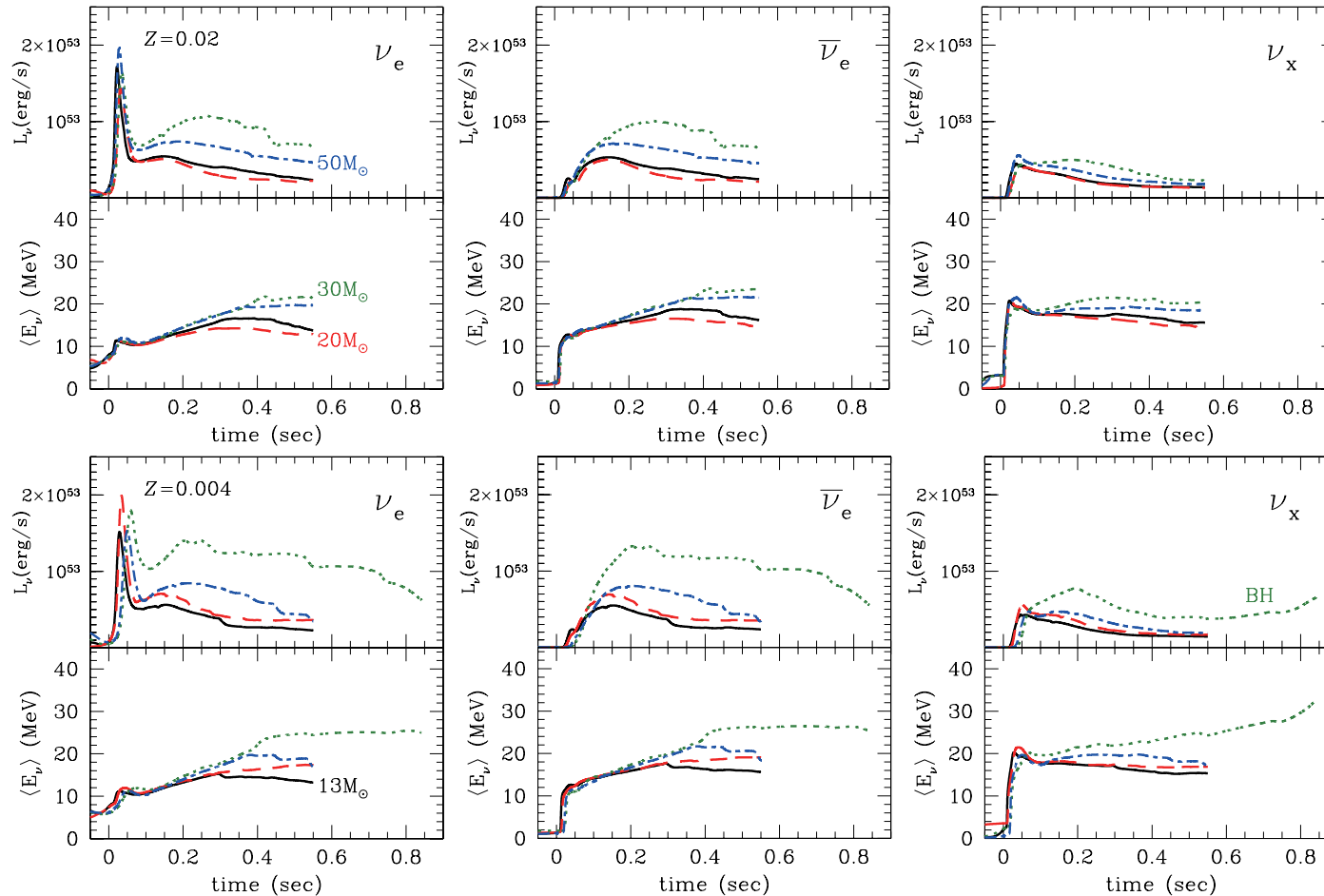
| 質量階層 | 物質効果による survival probability | |
|----------|--|--|
| | P | \bar{P} |
| normal | $\sin^2 \theta_{13} = 0.02 \sim 0$ | $\cos^2 \theta_{12} \cos^2 \theta_{13} = 0.68$ |
| inverted | $\sin^2 \theta_{12} \cos^2 \theta_{13} = 0.32$ | $\sin^2 \theta_{13} = 0.02 \sim 0$ |

新しい超新星ニュートリノデータベース

<http://asphwww.ph.noda.tus.ac.jp/snn/> Nakazato *et al.*, ApJS205 (2013) 2

数種類の親星モデル ($M = 13, 20, 30, 50M_{\odot}$, $Z = 0.02(Z_{\odot}), 0.004(0.2Z_{\odot})$)

重力崩壊、衝撃波の伝播段階からのニュートリノ (1D simulations: not explode)



general tendency

$$\begin{array}{rcl}
 \sigma_{\nu_e} & > & \sigma_{\bar{\nu}_e} & > & \sigma_{\nu_x} \\
 R_{\nu_e} & > & R_{\bar{\nu}_e} & > & R_{\nu_x} \\
 T_{\nu_e} & < & T_{\bar{\nu}_e} & < & T_{\nu_x} \\
 \langle \omega_{\nu_e} \rangle & < & \langle \omega_{\bar{\nu}_e} \rangle & < & \langle \omega_{\nu_x} \rangle
 \end{array}$$

$Z = 0.004, M = 30M_{\odot}$ は爆発せずブラックホール形成 (mass loss が少なく, 非常に重いコアが重力崩壊するケース)

Figure 12. Luminosities (upper plots) and average energies (lower plots) of the emitted neutrinos as a function of time after the bounce from the ν RHD simulations. The panels correspond, from left to right, to ν_e , $\bar{\nu}_e$, and ν_x ($= \nu_{\mu}, \nu_{\tau}, \bar{\nu}_{\mu}, \bar{\nu}_{\tau}$). The results for the models with metallicity $Z = 0.02$ are shown in the top panels, and those for the models with $Z = 0.004$ are shown in the bottom panels. In all panels, solid, dashed, dotted, and dot-dashed lines correspond to the models with initial mass $M_{\text{init}} = 13 M_{\odot}, 20 M_{\odot}, 30 M_{\odot}$, and $50 M_{\odot}$, respectively. “BH” means a black-hole-forming model with $M_{\text{init}} = 30 M_{\odot}$ and $Z = 0.004$; its end point corresponds to the moment of black hole formation.

Table 1
Key Parameters for All Models

| Z | M_{init} (M_{\odot}) | M_{tot} (M_{\odot}) | M_{He} (M_{\odot}) | M_{CO} (M_{\odot}) | M_{core} (M_{\odot}) | t_{revive} (ms) | $M_{b,\text{NS}}$ (M_{\odot}) | $M_{g,\text{NS}}$ (M_{\odot}) | $\langle E_{\nu_e} \rangle$ (MeV) | $\langle E_{\bar{\nu}_e} \rangle$ (MeV) | $\langle E_{\nu_x} \rangle$ (MeV) | $E_{\nu_e,\text{tot}}$ (10^{52} erg) | $E_{\bar{\nu}_e,\text{tot}}$ (10^{52} erg) | $E_{\nu_x,\text{tot}}$ (10^{52} erg) | $E_{\nu_{\text{all}},\text{tot}}$ (10^{53} erg) |
|-------|--------------------------------------|-------------------------------------|------------------------------------|------------------------------------|--------------------------------------|-----------------------------|--------------------------------------|--------------------------------------|--------------------------------------|--|--------------------------------------|--|--|--|---|
| 0.02 | 13 | 12.3 | 3.36 | 1.97 | 1.55 | 100 | 1.50 | 1.39 | 9.08 | 10.8 | 11.9 | 3.15 | 2.68 | 3.19 | 1.86 |
| | | | | | | 200 | 1.59 | 1.46 | 9.49 | 11.3 | 12.0 | 3.51 | 3.04 | 3.45 | 2.03 |
| | | | | | | 300 | 1.64 | 1.50 | 9.91 | 11.7 | 12.1 | 3.83 | 3.33 | 3.59 | 2.15 |
| | 20 | 17.8 | 5.01 | 3.33 | 1.56 | 100 | 1.47 | 1.36 | 9.00 | 10.7 | 11.8 | 3.03 | 2.56 | 3.06 | 1.78 |
| | | | | | | 200 | 1.54 | 1.42 | 9.32 | 11.1 | 11.9 | 3.30 | 2.82 | 3.27 | 1.92 |
| | | | | | | 300 | 1.57 | 1.45 | 9.57 | 11.4 | 12.0 | 3.49 | 3.00 | 3.35 | 1.99 |
| | 30 | 23.8 | 8.54 | 7.10 | 2.06 | 100 | 1.62 | 1.49 | 9.32 | 11.1 | 12.1 | 3.77 | 3.23 | 3.72 | 2.19 |
| | | | | | | 200 | 1.83 | 1.66 | 10.2 | 12.1 | 12.5 | 4.80 | 4.24 | 4.51 | 2.71 |
| | | | | | | 300 | 1.98 | 1.78 | 11.1 | 13.0 | 12.8 | 5.76 | 5.16 | 4.99 | 3.09 |
| 50 | 11.9 | ... | 11.9 | 1.89 | 100 | 1.67 | 1.52 | 9.35 | 11.0 | 12.1 | 3.76 | 3.24 | 3.85 | 2.24 | |
| | | | | | 200 | 1.79 | 1.63 | 9.98 | 11.7 | 12.3 | 4.39 | 3.85 | 4.28 | 2.53 | |
| | | | | | 300 | 1.87 | 1.69 | 10.6 | 12.4 | 12.4 | 4.95 | 4.38 | 4.51 | 2.74 | |
| 0.004 | 13 | 12.5 | 3.76 | 2.37 | 1.61 | 100 | 1.50 | 1.38 | 9.07 | 10.8 | 11.9 | 3.15 | 2.68 | 3.18 | 1.86 |
| | | | | | | 200 | 1.58 | 1.45 | 9.47 | 11.3 | 12.0 | 3.51 | 3.03 | 3.45 | 2.03 |
| | | | | | | 300 | 1.63 | 1.49 | 9.76 | 11.6 | 12.1 | 3.75 | 3.26 | 3.57 | 2.13 |
| | 20 | 18.9 | 5.18 | 3.43 | 1.76 | 100 | 1.63 | 1.49 | 9.28 | 11.0 | 12.0 | 3.68 | 3.12 | 3.72 | 2.17 |
| | | | | | | 200 | 1.73 | 1.57 | 9.71 | 11.4 | 12.2 | 4.11 | 3.55 | 4.04 | 2.38 |
| | | | | | | 300 | 1.77 | 1.61 | 10.1 | 11.9 | 12.3 | 4.43 | 3.84 | 4.20 | 2.51 |
| | 30 | 26.7 | 11.1 | 9.35 | 2.59 | ... | ... | ... | 17.5 | 21.7 | 23.4 | 9.49 | 8.10 | 4.00 | 3.36 |
| | 50 | 16.8 | ... | 16.8 | 1.95 | 100 | 1.67 | 1.52 | 9.10 | 10.9 | 12.0 | 3.83 | 3.19 | 3.81 | 2.23 |
| | | | | | | 200 | 1.79 | 1.63 | 9.77 | 11.7 | 12.3 | 4.54 | 3.89 | 4.30 | 2.56 |
| | | | | | | 300 | 1.91 | 1.72 | 10.5 | 12.5 | 12.5 | 5.20 | 4.51 | 4.61 | 2.81 |

Notes. M_{init} and Z are the initial mass and metallicity of progenitors, respectively. M_{tot} , M_{He} , and M_{CO} are the total progenitor mass, He core mass, and CO core mass when the collapse begins, respectively. Since models with $M_{\text{init}} = 50 M_{\odot}$ become Wolf–Rayet stars, M_{He} is not defined and M_{CO} equals M_{tot} . M_{core} is a core mass defined as the region of oxygen depletion. t_{revive} is the shock revival time. $M_{b,\text{NS}}$ and $M_{g,\text{NS}}$ are the baryonic mass and gravitational mass of the remnant neutron states, respectively. The mean energy of emitted ν_i until 20 s after the bounce is denoted as $\langle E_{\nu_i} \rangle \equiv E_{\nu_i,\text{tot}}/N_{\nu_i,\text{tot}}$, where $E_{\nu_i,\text{tot}}$ and $N_{\nu_i,\text{tot}}$ are the total energy and number of neutrinos, respectively. ν_x stands for μ - and τ -neutrinos and their anti-particles: $E_{\nu_x} = E_{\nu_{\mu}} = E_{\bar{\nu}_{\mu}} = E_{\nu_{\tau}} = E_{\bar{\nu}_{\tau}}$. $E_{\nu_{\text{all}},\text{tot}}$ is the total of neutrino energy summed over all species. The model with $M_{\text{init}} = 30 M_{\odot}$ and $Z = 0.004$ is a black-hole-forming model, for which mean and total neutrino energies emitted up to the black hole formation are shown.

原始中性子星冷却段階からのニュートリノ

初期モデル = 動的シミュレーションの仮定した衝撃波復活時間 t_{rev} におけるショックフロント内を切り出す (非球対称効果で衝撃波が復活して爆発すれば、衝撃波を覆っていた層は吹き飛ば)

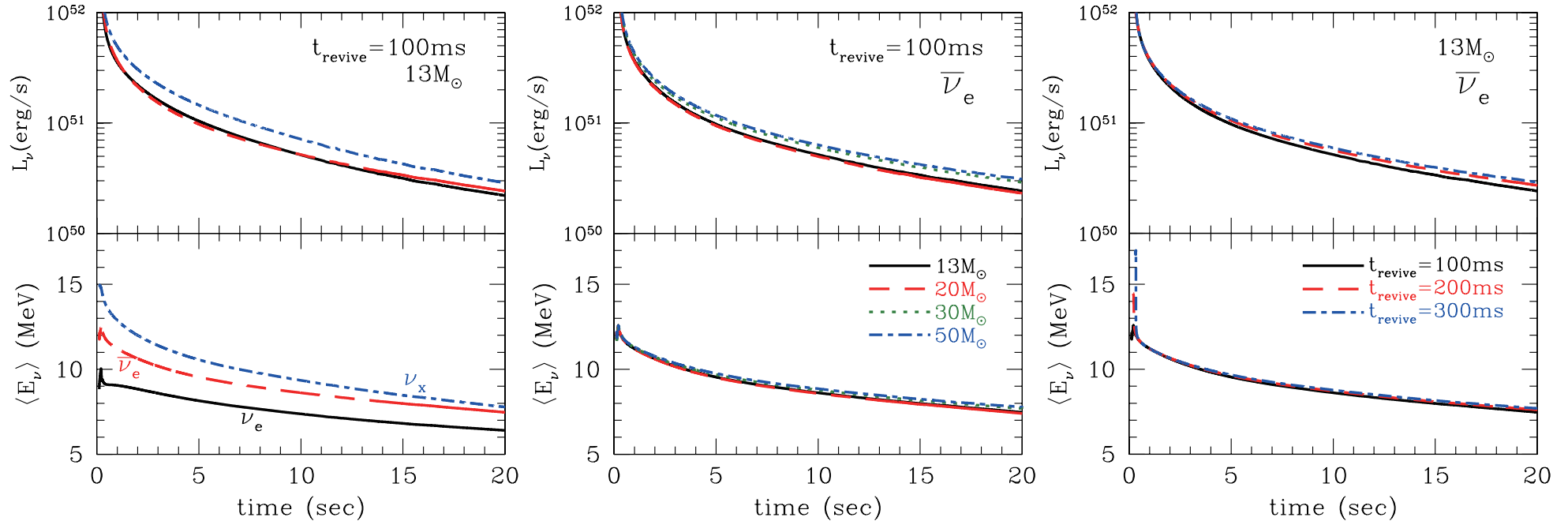


Figure 13. Same as Figure 12 but from the PNSC simulations. In the left panel, signals of ν_e (solid lines), $\bar{\nu}_e$ (dashed lines), and ν_x (dot-dashed lines) are shown for the model with $(M_{\text{init}}, Z, t_{\text{revive}}) = (13 M_\odot, 0.02, 100 \text{ ms})$. In the central panel, $\bar{\nu}_e$ signals are shown for the models with $(Z, t_{\text{revive}}) = (0.02, 100 \text{ ms})$ and $M_{\text{init}} = 13 M_\odot$ (solid lines), $20 M_\odot$ (dashed lines), $30 M_\odot$ (dotted lines), and $50 M_\odot$ (dot-dashed lines). In the right panel, $\bar{\nu}_e$ signals are shown for the models with $(M_{\text{init}}, Z) = (13 M_\odot, 0.02)$ and $t_{\text{revive}} = 100 \text{ ms}$ (solid lines), 200 ms (dashed lines), and 300 ms (dot-dashed lines).

動的段階と準静的段階の接続

$$F_{\nu_i}(E, t) = F_{\nu_i}^{\text{acc}}(E, t) + F_{\nu_i}^{\text{PNSC}}(E, t) \sim f(t)F_{\nu_i}^{\text{dyn}}(E, t) + (1 - f(t))F_{\nu_i}^{\text{PNSC}}(E, t)$$

$$F_{\nu_i}^{\text{acc}}(\text{explosion}) = f(t)F_{\nu_i}^{\text{acc, max}} = f(t)(F_{\nu_i}^{\text{dyn}}(\text{no explosion}) - F_{\nu_i}^{\text{PNSC}}(\text{no accretion}))$$

$$f(t) \equiv \begin{cases} 1 & t < t_{\text{rev}} + t_{\text{shift}} \\ \exp\left(-\frac{t - (t_{\text{rev}} + t_{\text{shift}})}{\tau_{\text{decay}}}\right) & t > t_{\text{rev}} + t_{\text{shift}} \end{cases} \quad \tau_{\text{decay}} = 30\text{ms}, t_{\text{shift}} = 50\text{ms}$$

モデルパラメーター: 衝撃波復活時間 (t_{rev})

ニュートリノ対流が効果的に働いて爆発するケース \rightarrow small t_{rev}

一方、SASI が爆発にとって重要な役割を果たすなら、SASI の成長に時間がかかるので large t_{rev}

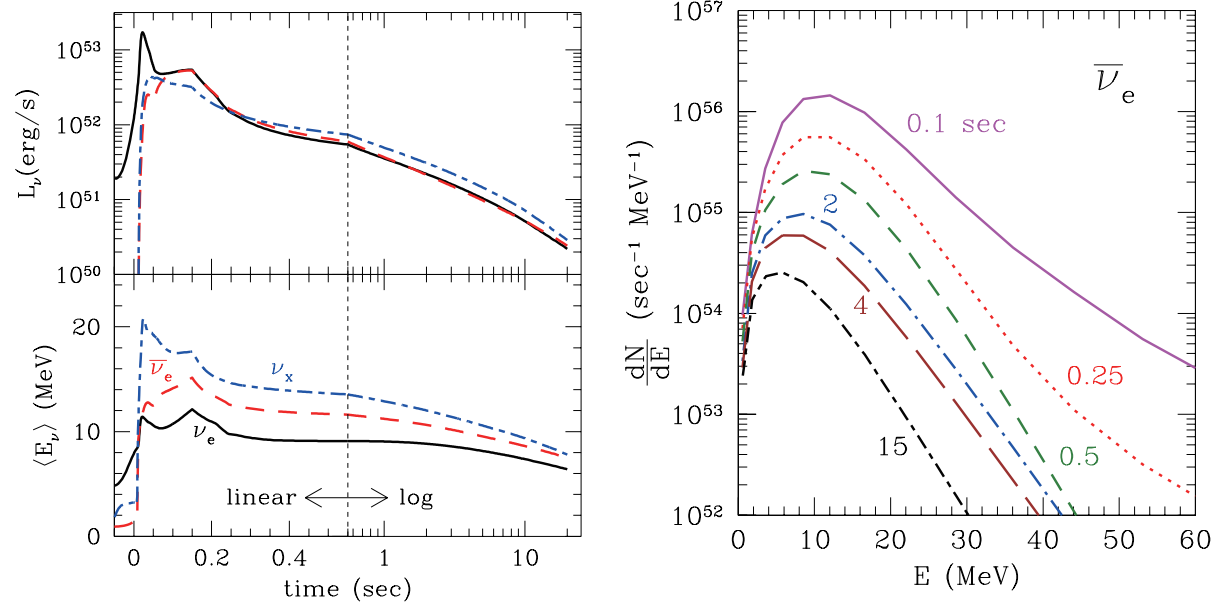
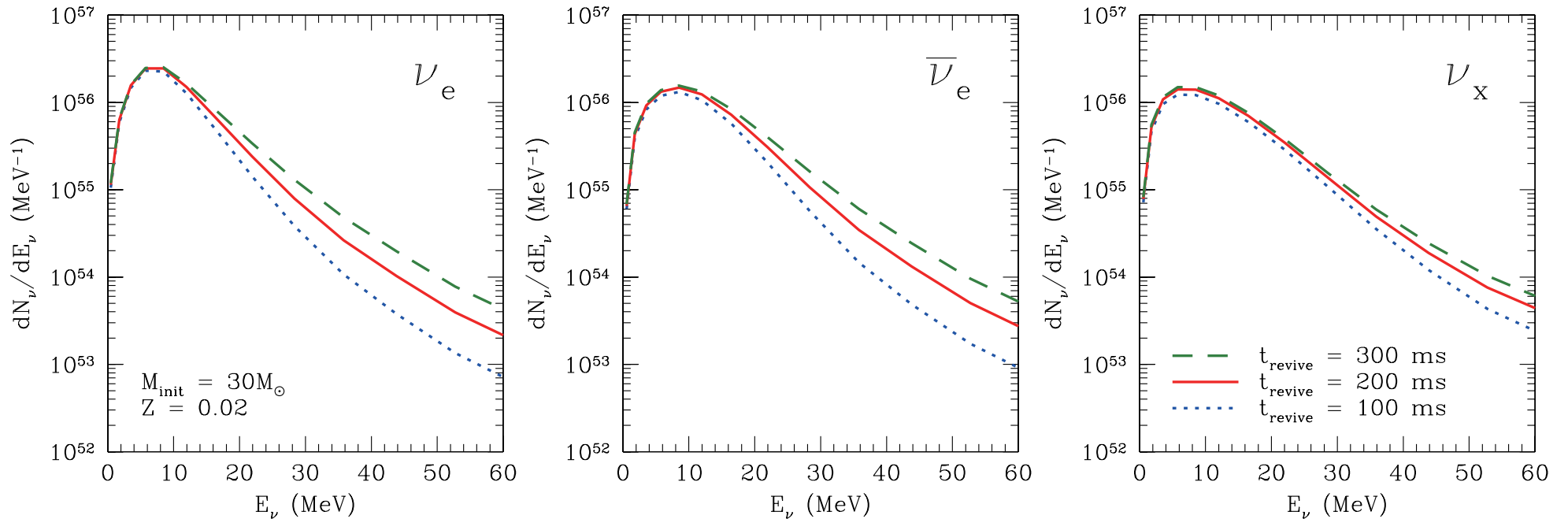


Figure 14. Time evolution of neutrino luminosity and average energy (left) and number spectrum of $\bar{\nu}_e$ (right) from ν RHD and PNSC simulations with the interpolation (13) for the model with $(M_{\text{init}}, Z, t_{\text{rev}}) = (13 M_\odot, 0.02, 100 \text{ ms})$. In the left panel, solid, dashed, and dot-dashed lines represent ν_e , $\bar{\nu}_e$, and ν_x (dot-dashed lines), respectively. In the right panel, the lines correspond, from top to bottom, to 0.1, 0.25, 0.5, 2, 4, and 15 s after the bounce.

$$13M_\odot, Z = 0.02, t_{\text{rev}} = 100 \text{ ms}$$

衝撃波復活時間の影響

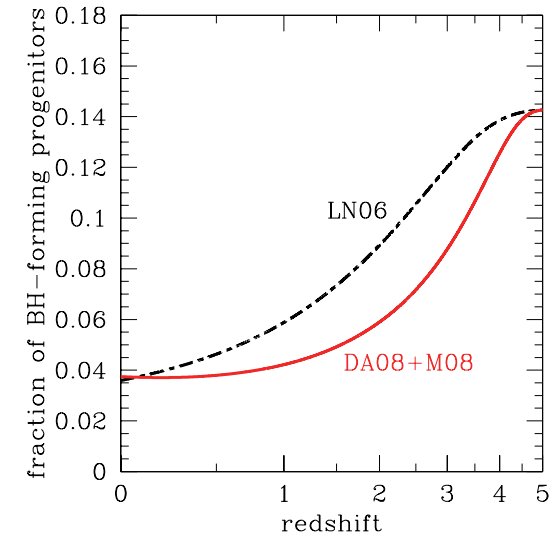
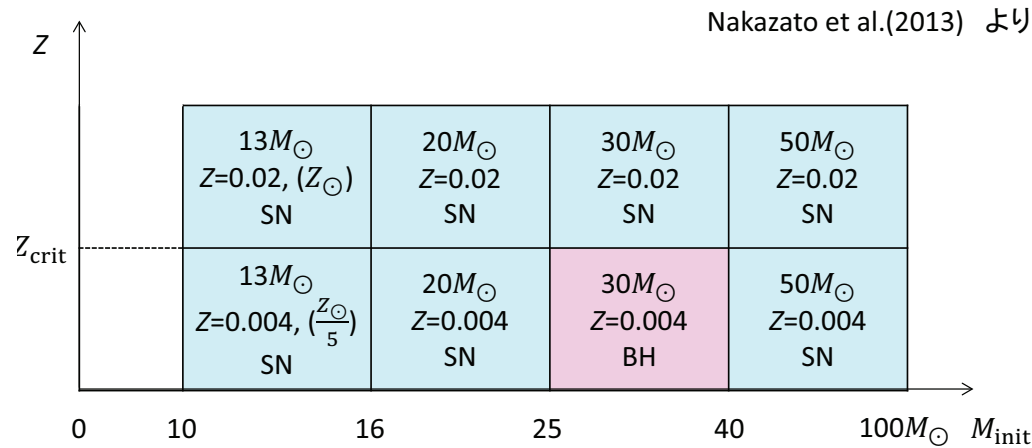


Neutrino number spectra of supernova with $30M_\odot$, $Z = 0.02$ and shock revival times of $t_{\text{revive}} = 100$ ms (dotted), 200 ms (solid) and 300 ms (dashed). The left, central and right panels correspond to ν_e , $\bar{\nu}_e$ and ν_x ($= \nu_\mu = \bar{\nu}_\mu = \nu_\tau = \bar{\nu}_\tau$), respectively.

衝撃波の復活まで accretion phase が続くため、衝撃波復活時間が遅いほど放出される accretion 起源の高エネルギーニュートリノが多くなる。

ブラックホール形成イベントの影響

$M = 30M_{\odot}$, $Z = 0.004$: mass loss が少なくコアの質量が非常に大きいので、爆発せずブラックホールになると考えられる。



ブラックホール形成イベントの割合

Fraction of black-hole-forming progenitors as a function of redshift. Dot-dashed and solid lines correspond to the models with the metallicity evolution of LN06 and DA08+M08, respectively. $Z_{\text{crit}} \equiv \sqrt{Z_{\odot} \cdot 0.2Z_{\odot}}$

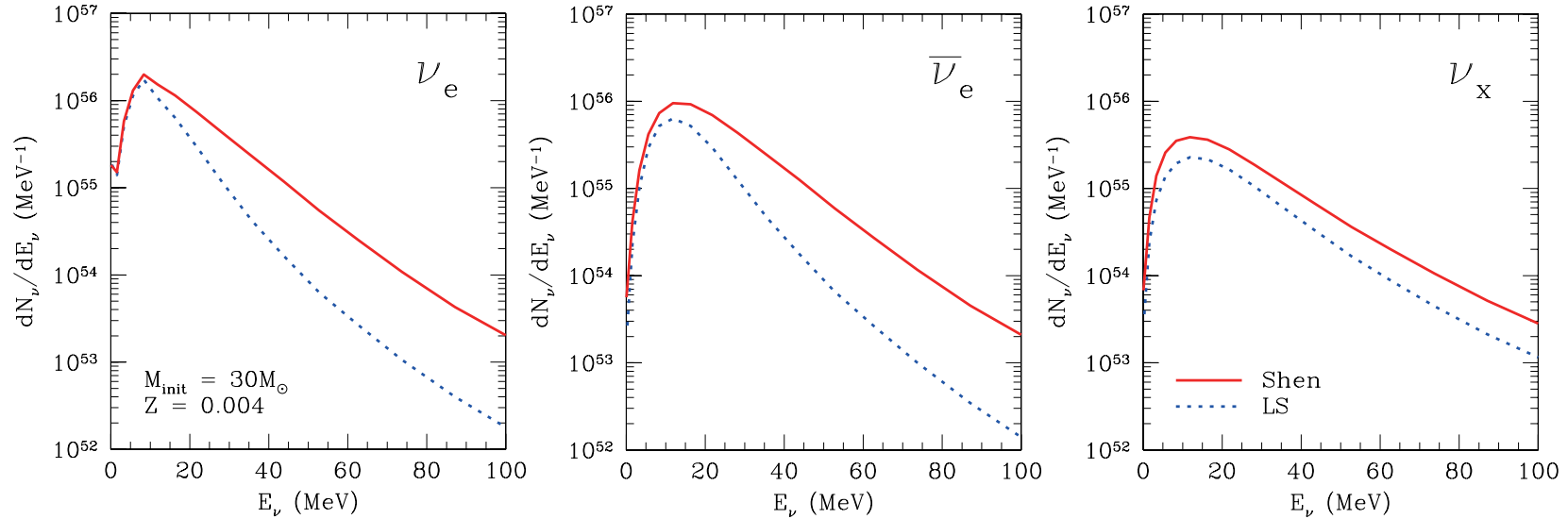
ブラックホール形成イベントに対する状態方程式の影響

TABLE 1

NUMERICAL RESULTS FOR BLACK HOLE FORMATION OF PROGENITOR WITH $(M, Z) = (30M_{\odot}, 0.004)$.

| EOS | t_{BH} (ms) | $\langle E_{\nu_e} \rangle$ (MeV) | $\langle E_{\bar{\nu}_e} \rangle$ (MeV) | $\langle E_{\nu_x} \rangle$ (MeV) | $E_{\nu_e, \text{tot}}$ (10^{52} erg) | $E_{\bar{\nu}_e, \text{tot}}$ (10^{52} erg) | $E_{\nu_x, \text{tot}}$ (10^{52} erg) | $E_{\nu_{\text{all}}, \text{tot}}$ (10^{53} erg) |
|-------------|-------------------------|--------------------------------------|--|--------------------------------------|---|---|---|--|
| Shen | 842 | 17.5 | 21.7 | 23.4 | 9.49 | 8.10 | 4.00 | 3.36 |
| LS(220 MeV) | 342 | 12.5 | 16.4 | 22.3 | 4.03 | 2.87 | 2.11 | 1.53 |

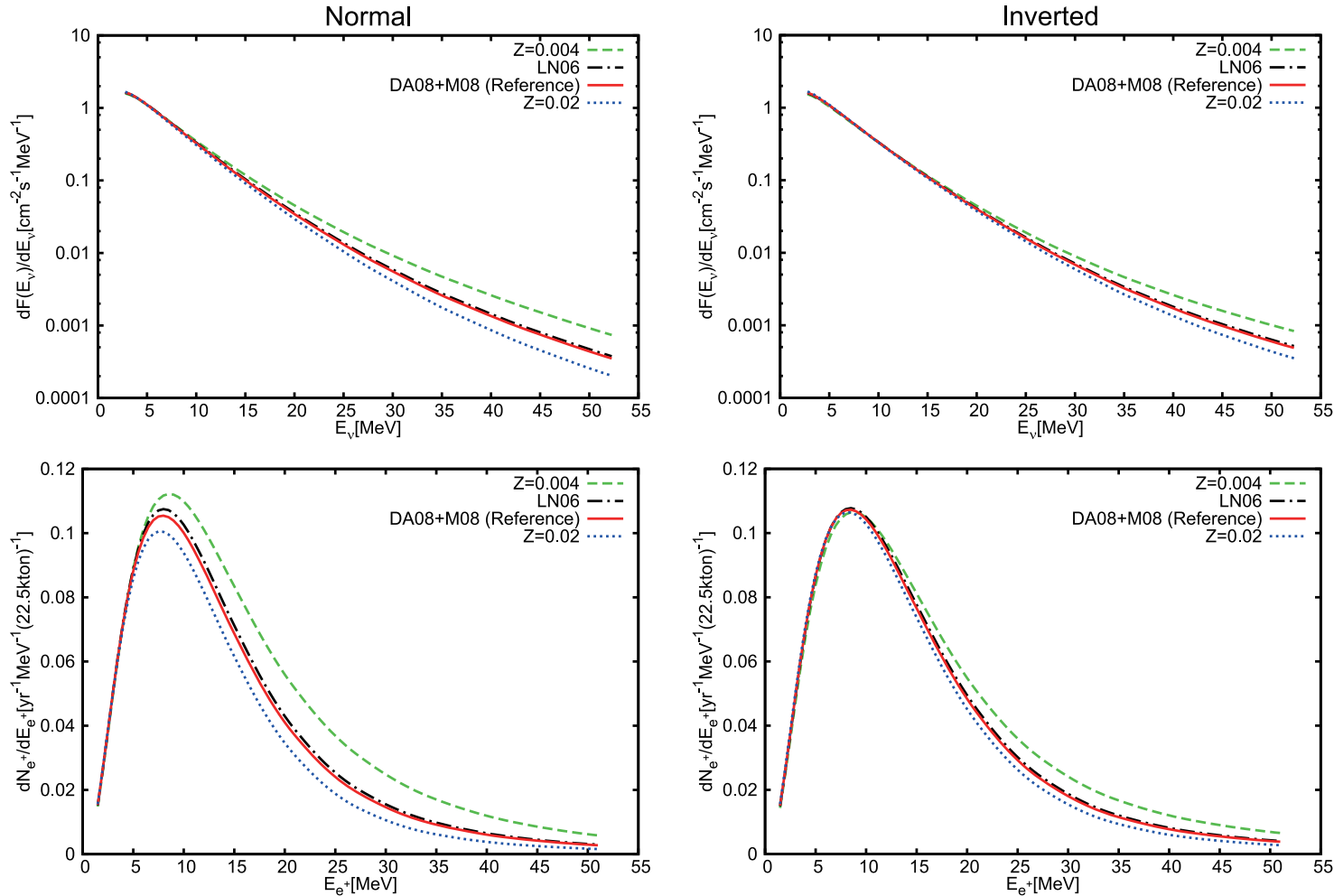
NOTE. — t_{BH} is the time to black hole formation measured from the core bounce. The mean energy of the emitted ν_i until black hole formation is denoted as $\langle E_{\nu_i} \rangle \equiv E_{\nu_i, \text{tot}}/N_{\nu_i, \text{tot}}$, where $E_{\nu_i, \text{tot}}$ and $N_{\nu_i, \text{tot}}$ are the total energy and number of neutrinos, respectively. ν_x stands for μ - and τ -neutrinos and their anti-particles: $E_{\nu_x} = E_{\nu_{\mu}} = E_{\bar{\nu}_{\mu}} = E_{\nu_{\tau}} = E_{\bar{\nu}_{\tau}}$. $E_{\nu_{\text{all}}, \text{tot}}$ is the total neutrino energy summed over all species.



Neutrino number spectra for black hole formation with $30M_{\odot}$, $Z = 0.004$ and Shen EOS (solid) and LS EOS (dotted). The left, central and right panels correspond to ν_e , $\bar{\nu}_e$ and ν_x ($= \nu_{\mu} = \bar{\nu}_{\mu} = \nu_{\tau} = \bar{\nu}_{\tau}$), respectively.

柔らかい LS EOS では中性子星の最大質量が小さく早くブラックホールになってしまうため、accretion phase が短く放出されるニュートリノも少ない。

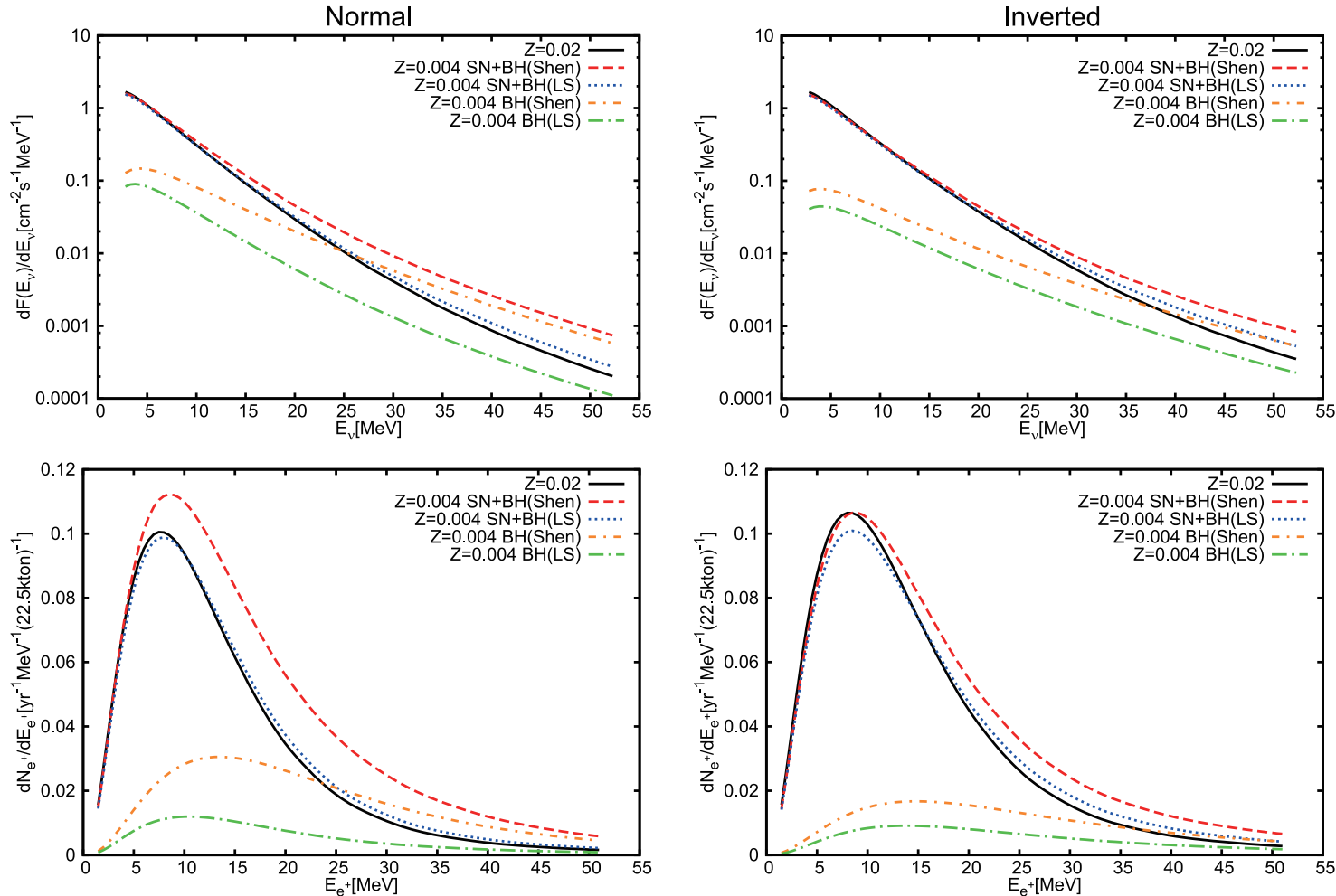
金属量進化の影響



BH 形成イベント
(高エネルギー $\bar{\nu}_e$
多) が多いモデル
で、 $\bar{\nu}_e$ が 68% 生き
残る normal hier-
archy の場合は、
SRN が特に多くな
る。
DA08+M08 と
LN06 との差は小
さい。

Fluxes of SRNs (*upper panels*) and event rate spectra in Super-Kamiokande over 1 year (*lower panels*) obtained using models with CSFRD of DA08, shock revival time of $t_{\text{revive}} = 200$ ms and Shen EOS. The left and right panels show the results for the normal and inverted mass hierarchies, respectively. Solid and dot-dashed lines correspond to models with the metallicity evolutions of DA08+M08 and LN06, respectively, while other lines denote the results for fixed metallicity with $Z = 0.02$ (dotted) and 0.004 (dashed).

状態方程式の影響

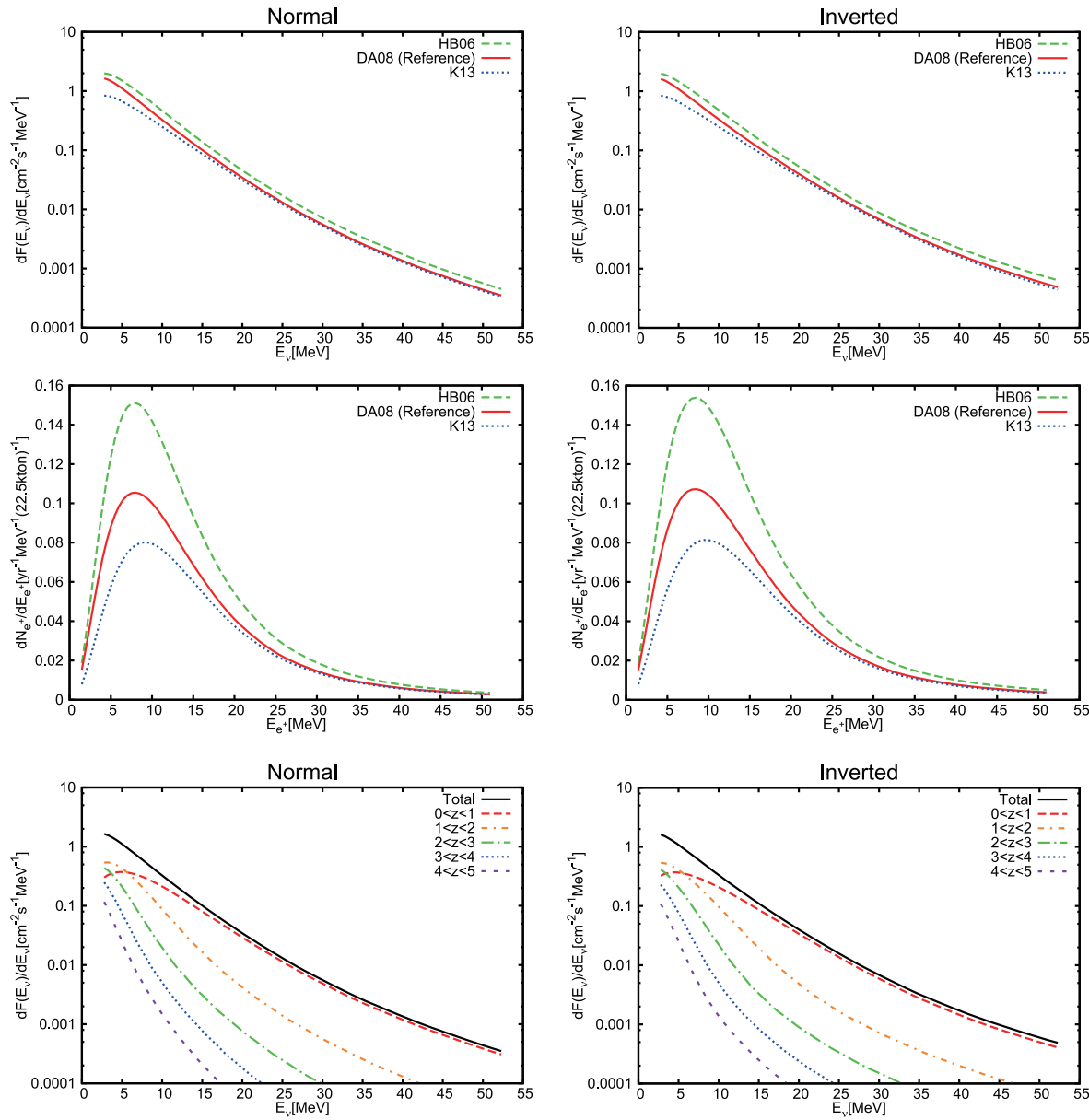


柔らかい EOS で
ブラックホールに
なるケースは、早
くブラックホール
になってしまい、
ニュートリノの放
出量が少ないので、
SRN への寄与が小
さい。

Same as Figure 7 but for different EOS. Dashed and dotted lines correspond to models with the Shen EOS and LS EOS, respectively, with the metallicity fixed to $Z = 0.004$. The contribution of black-hole-forming failed supernovae is extracted for the Shen EOS (dot-short-dashed) and LS EOS (dot-long-dashed). Solid lines denote the results for fixed metallicity with $Z = 0.02$, where failed supernovae are not included.

金属量進化がないとして、EOS によって BH 形成イベントの寄与がどう変わるか

星形成率密度 CSFRD の影響

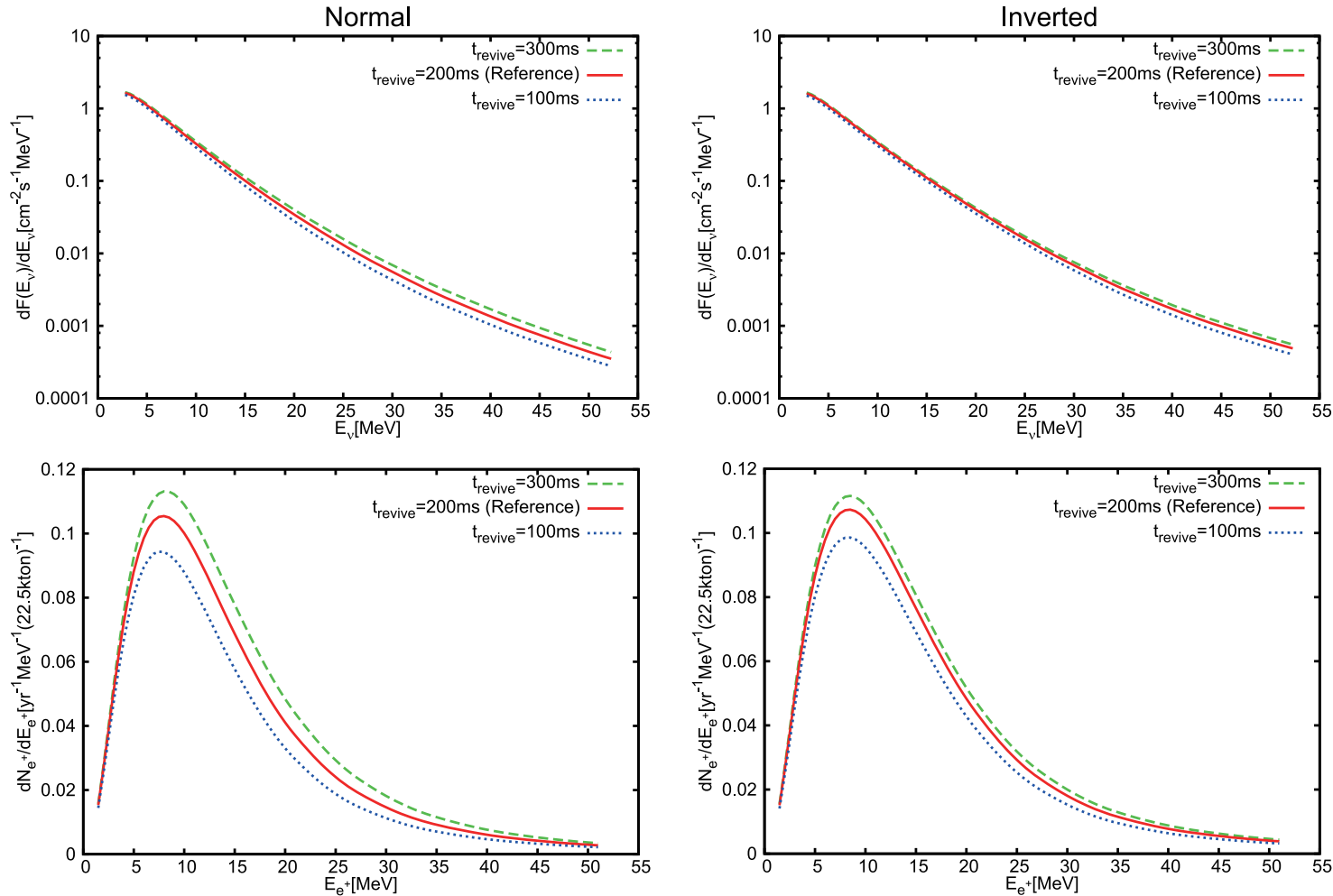


$z > 0.5$ において、CSFRD のモデル差が大きくなるので、低エネルギー SRN に影響がでる。

Same as Figure 7 but for the models with metallicity evolution of DA08+M08, shock revival time of $t_{\text{revive}} = 200$ ms and Shen EOS. Dashed, solid and dotted lines correspond to models with the CSFRD of HB06, DA08 and K13, respectively.

0 < z < 1, 1 < z < 2, 2 < z < 3, 3 < z < 4, 4 < z < 5 からの寄与

衝撃波復活時間の影響



accretion が長く
 続くモデルほど、
 SRN が多くなり、
 $\bar{\nu}_e$ が 68% 生き残る
 normal hierarchy
 は差が顕著

Same as Figure 7 but for models with CSFRD of DA08 and metallicity evolution of DA08+M08 and Shen EOS. Dotted, solid and dashed lines correspond to models with shock revival times of $t_{\text{revive}} = 100, 200$ and 300 ms, respectively.

TABLE 3

SRN EVENT RATES IN VARIOUS RANGES OF POSITRON ENERGY IN SUPER-KAMIOKANDE OVER 1 YEAR (I.E., PER 22.5 KTON YEAR) FOR MODELS WITH METALLICITY EVOLUTION OF DA08+M08.

| CSFRD | t_{revive} | EOS for BH | Normal mass hierarchy | | | Inverted mass hierarchy | | | Figure 12 |
|-------|---------------------|------------|-----------------------|-------|-----------|-------------------------|-------|-----------|-----------|
| | | | 18-26 | 10-18 | 10-26 MeV | 18-26 | 10-18 | 10-26 MeV | |
| HB06 | 100 ms | Shen | 0.286 | 0.704 | 0.990 | 0.375 | 0.832 | 1.207 | Maximum |
| | | LS | 0.227 | 0.635 | 0.863 | 0.351 | 0.806 | 1.156 | |
| | 200 ms | Shen | 0.361 | 0.833 | 1.193 | 0.429 | 0.920 | 1.349 | |
| | | LS | 0.302 | 0.764 | 1.066 | 0.404 | 0.893 | 1.297 | |
| | 300 ms | Shen | 0.432 | 0.938 | 1.370 | 0.463 | 0.967 | 1.431 | |
| | | LS | 0.374 | 0.869 | 1.242 | 0.439 | 0.941 | 1.379 | |
| DA08 | 100 ms | Shen | 0.219 | 0.515 | 0.734 | 0.286 | 0.598 | 0.885 | Reference |
| | | LS | 0.178 | 0.464 | 0.642 | 0.269 | 0.578 | 0.847 | |
| | 200 ms | Shen | 0.274 | 0.604 | 0.879 | 0.326 | 0.660 | 0.986 | |
| | | LS | 0.233 | 0.554 | 0.787 | 0.308 | 0.640 | 0.948 | |
| | 300 ms | Shen | 0.326 | 0.677 | 1.003 | 0.350 | 0.694 | 1.044 | |
| | | LS | 0.285 | 0.627 | 0.911 | 0.333 | 0.674 | 1.007 | |
| K13 | 100 ms | Shen | 0.203 | 0.443 | 0.645 | 0.264 | 0.505 | 0.769 | Minimum |
| | | LS | 0.171 | 0.410 | 0.581 | 0.252 | 0.492 | 0.744 | |
| | 200 ms | Shen | 0.252 | 0.514 | 0.767 | 0.298 | 0.554 | 0.853 | |
| | | LS | 0.221 | 0.482 | 0.703 | 0.286 | 0.542 | 0.827 | |
| | 300 ms | Shen | 0.298 | 0.570 | 0.868 | 0.319 | 0.580 | 0.899 | |
| | | LS | 0.266 | 0.537 | 0.804 | 0.306 | 0.568 | 0.874 | |

モデルのまとめ

- Reference
- 下限
- 上限

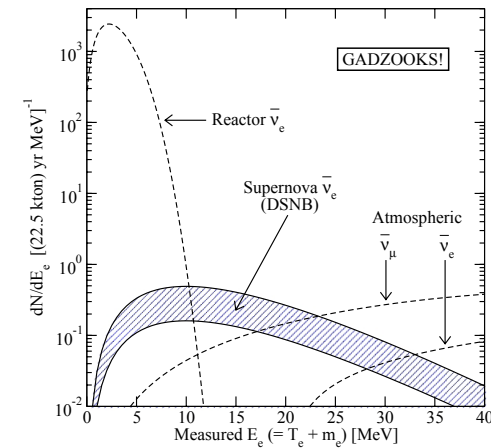
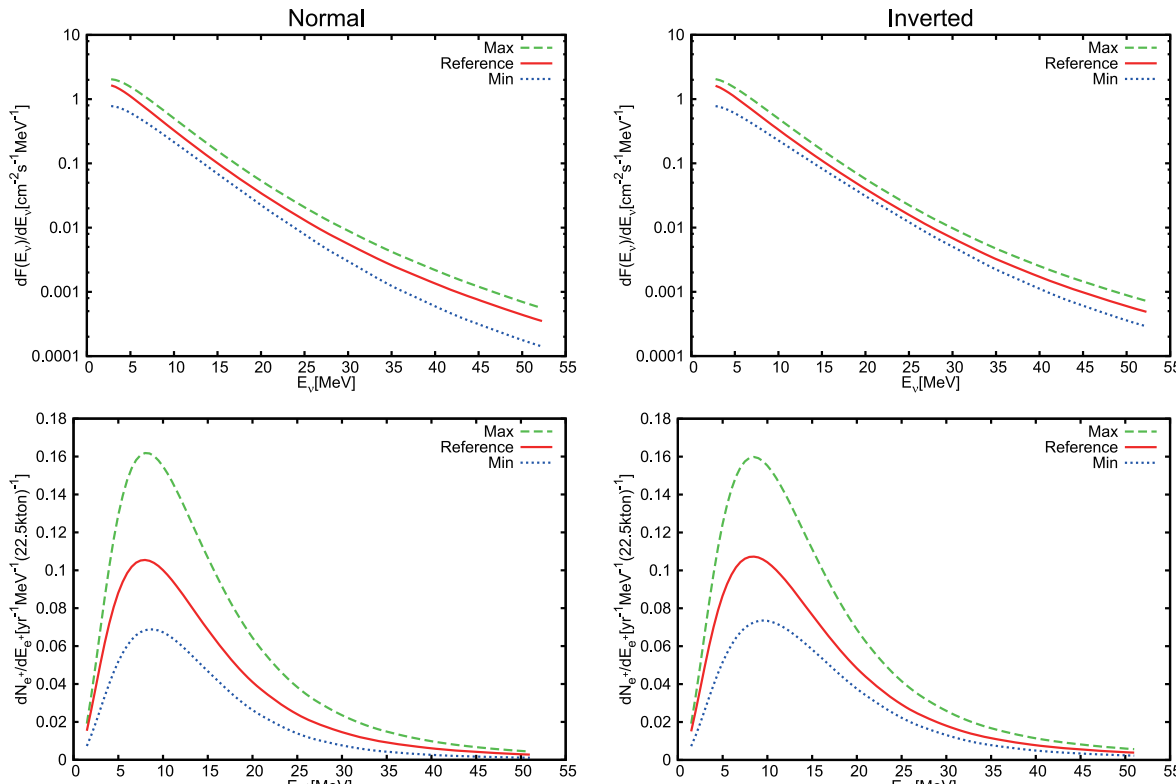
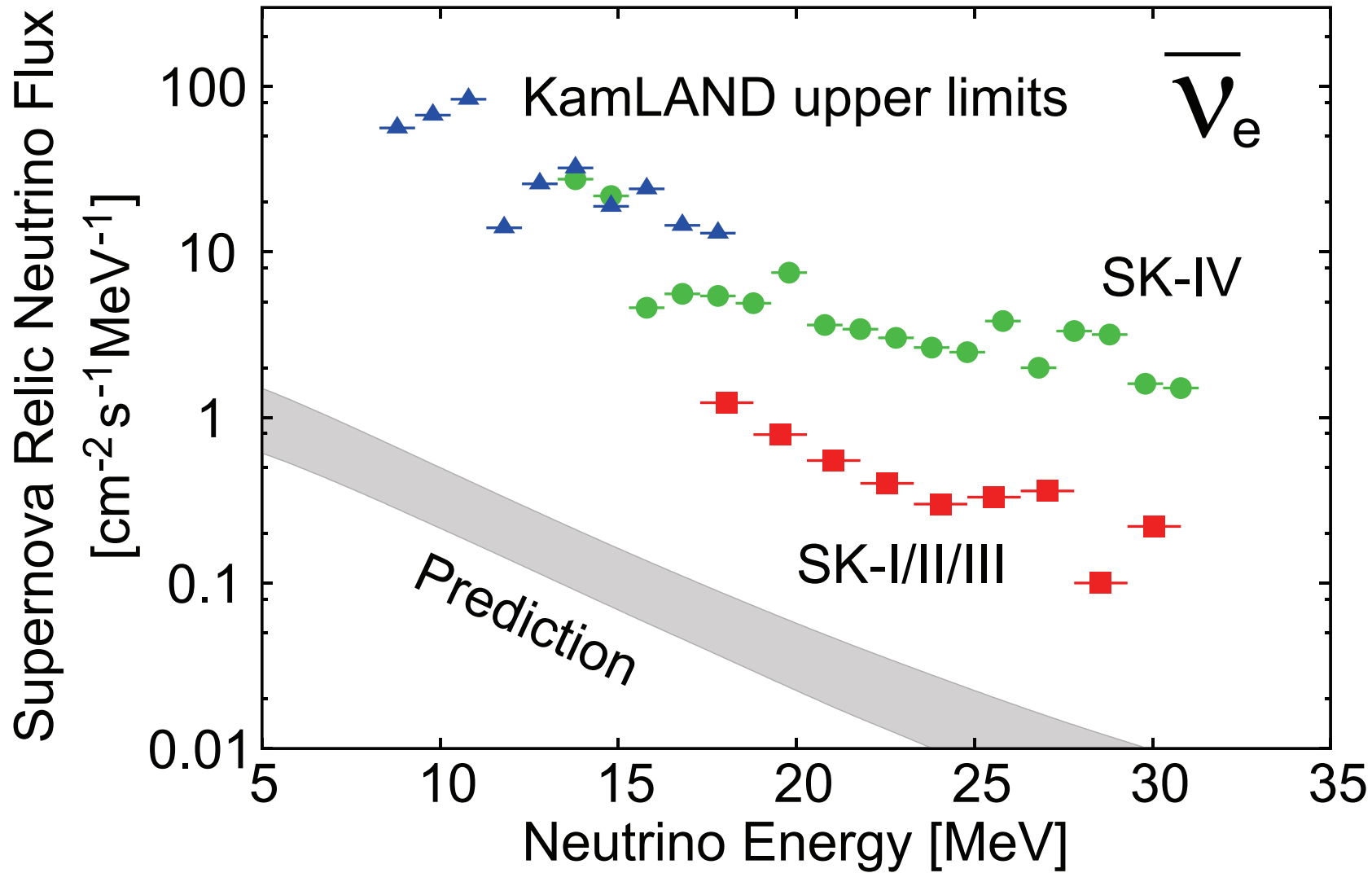
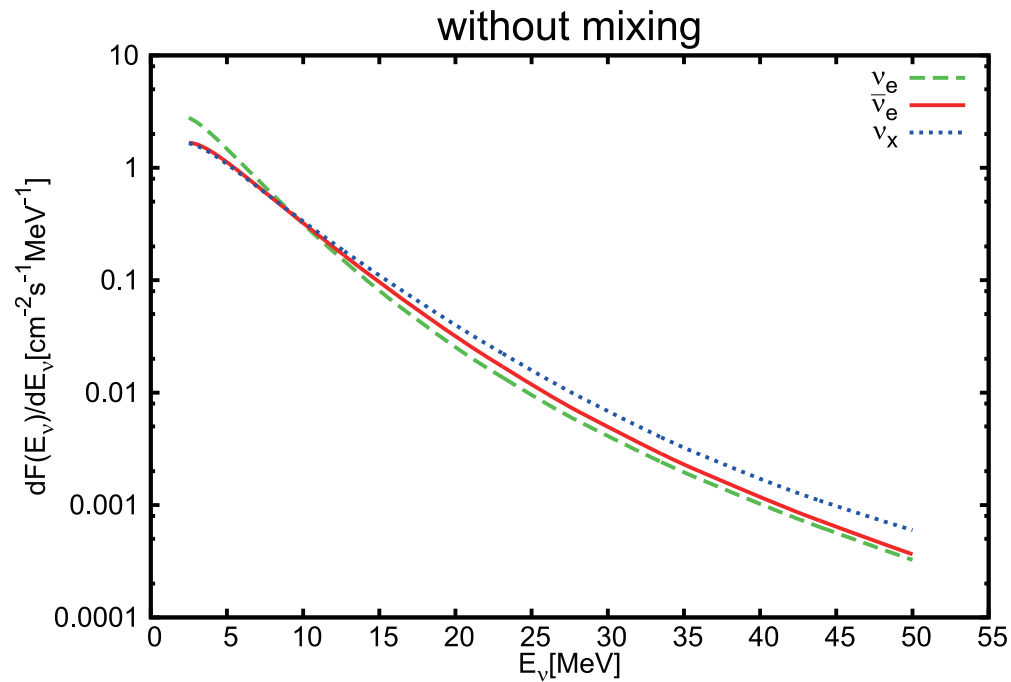
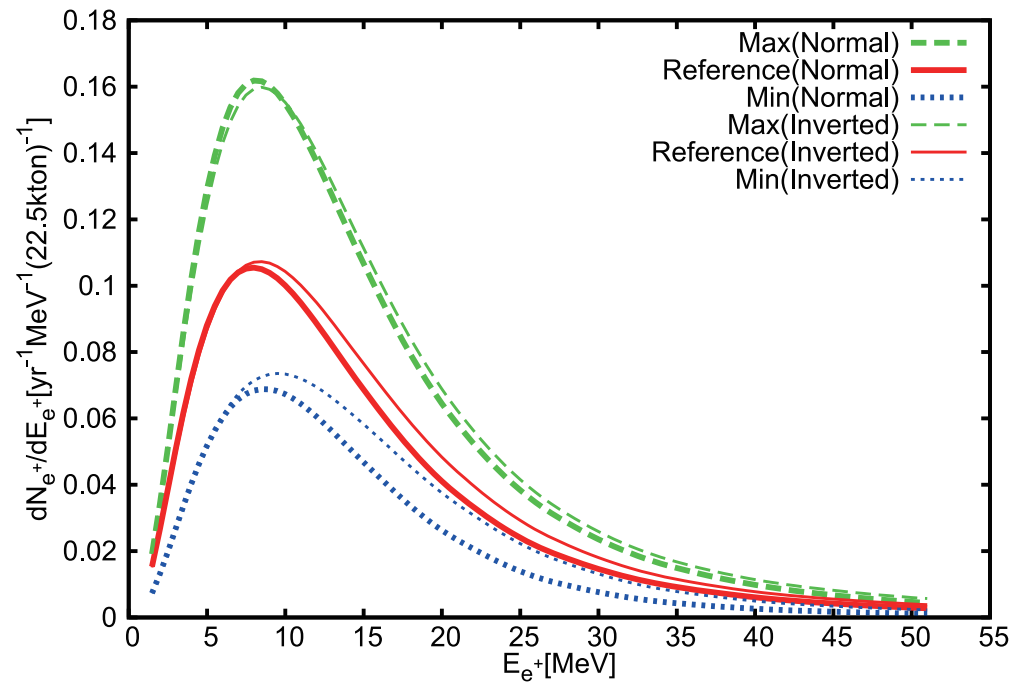


Figure 2. The expected coincident signals in Super-K with 100 tons of GdCl_3 . Detector energy resolution is properly taken into account. The upper supernova curve is the current SK relic limit, while the lower curve is the theoretical lower bound.



90% C.L. differential upper limits on $\bar{\nu}_e$ flux of SRNs. The squares, circles and triangles are results for Super-Kamiokande, Super-Kamiokande with a neutron-tagging and KamLAND. Dashed and dotted lines correspond to our theoretical models with maximum and minimum values of SRN event rate, respectively.

ニュートリノ振動の影響



低エネルギーニュートリノの観測ができれば...

ダークエネルギーモデルと SRN (Ono and Suzuki'07)

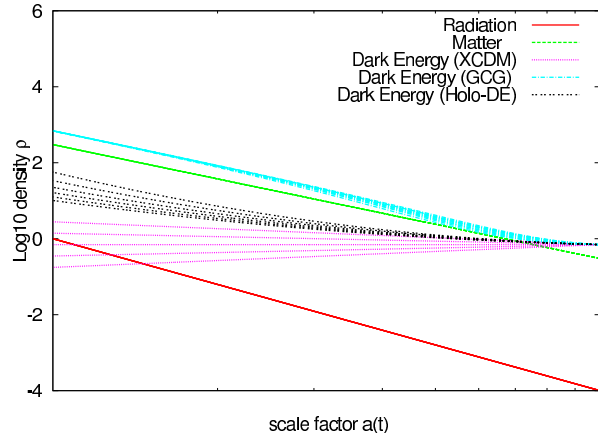


図 6: $\rho_X, \rho_{gcg}, \rho_{holo}$ とスケール因子 $a(t)$ との関係。

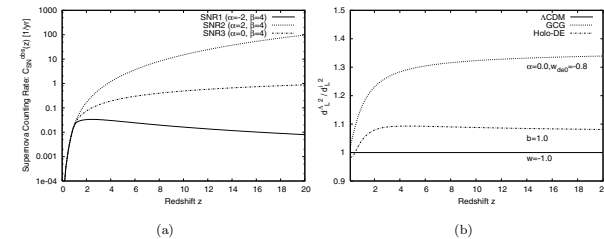
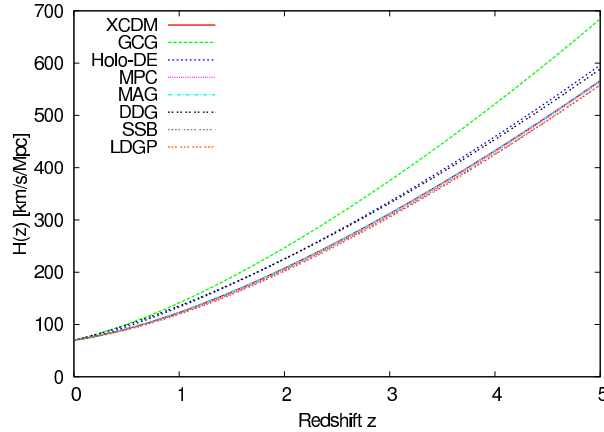


Fig. 3. (a) shows supernova counting rate models: SNR1 ($\alpha = -2, \beta = 4$), SNR2 ($\alpha = 2, \beta = 4$), SNR3 ($\alpha = 0, \beta = 4$). (b) shows dark energy model dependencies of d_L (the ratio to d_L of Λ CDM model).

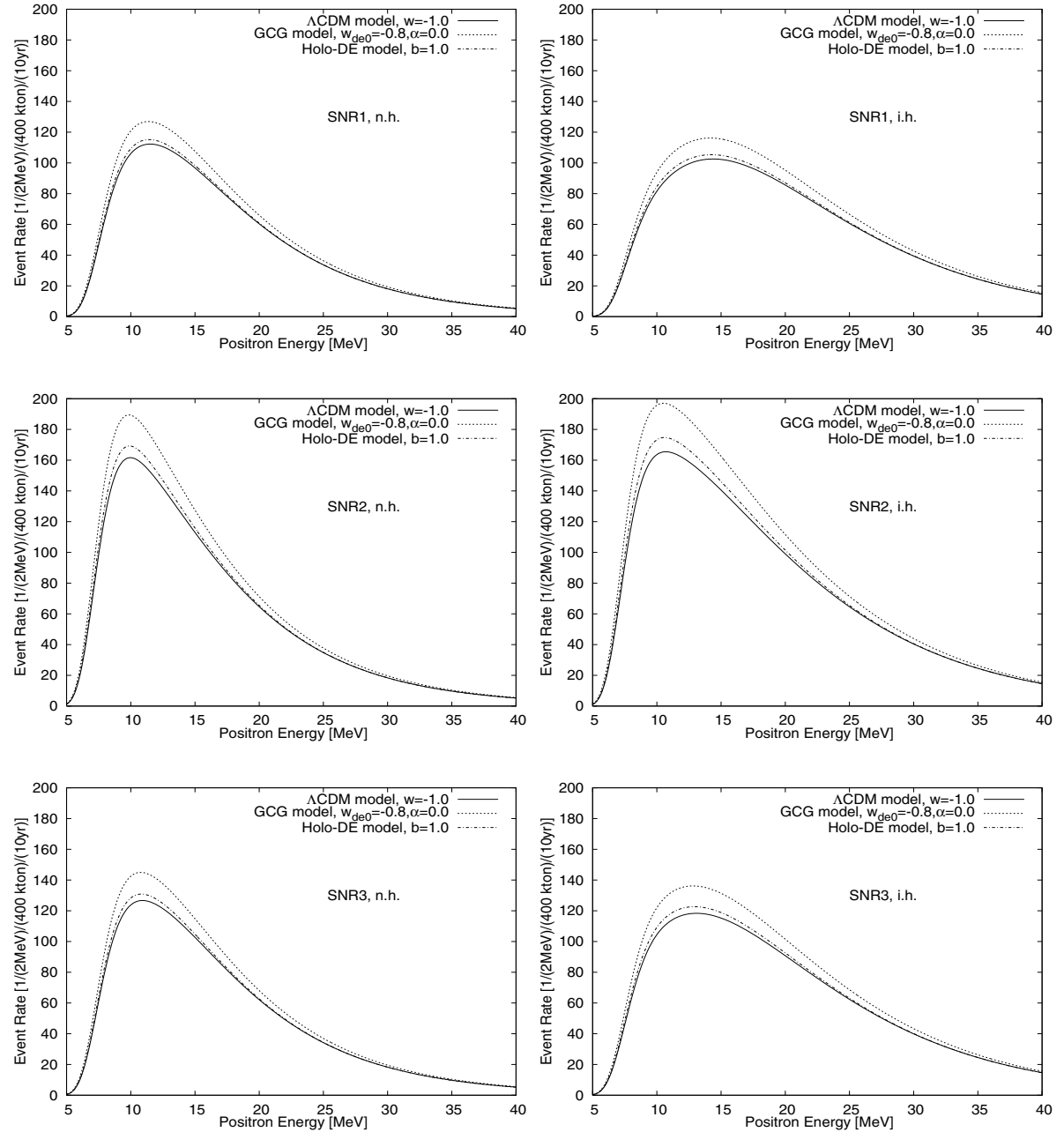


Fig. 4. Comparison of the predicted SRN event rate at HK with Gd for Λ CDM, GCG, holographic dark energy models. Supernova rate models are SNR1 (top panels), SNR2 (middle panels), SNR3 (bottom panels). The left and right panels show normal hierarchy (n.h.) $\bar{\nu}_e$ spectra and inverted hierarchy (i.h.) $\bar{\nu}_e$ spectra, respectively.

Summary

- ブラックホール形成イベントに起因する成分も含め、SRN に対する金属量進化、星形成率密度、衝撃波復活時間、状態方程式の影響を調べた。
- 衝撃波復活時間と状態方程式の影響は、高エネルギー成分に現れる。特に normal hierarchy の場合。
- 星形成率密度の影響は、低エネルギー成分に現れる。
- SK with Gd: 10 年で 4 - 9 SRN events(10-18MeV) が期待される。
- データ公開中

超新星ニュートリノ <http://asphwww.ph.noda.tus.ac.jp/snn/>

超新星背景ニュートリノ <http://asphwww.ph.noda.tus.ac.jp/srn/>